Defence Science Journal, Vol. 59, No. 6, November 2009, pp. 650-658

Microelectromechnical Systems Inertial Measurement Unit Error Modelling and Error Analysis for Low-cost Strapdown Inertial Navigation System

R. Ramalingam*, G. Anitha* and J. Shanmugam**

*Madras Institute of Technology, Anna University, Chrompet, Chennai - 600 044
**Tagore Engineering College, Vandalur, Chennai - 600 048

ABSTRACT

This paper presents error modelling and error analysis of microelectromechnical systems (MEMS) inertial measurement unit (IMU) for a low-cost strapdown inertial navigation system (INS). The INS consists of IMU and navigation processor. The IMU provides acceleration and angular rate of the vehicle in all the three axes. In this paper, errors that affect the MEMS IMU, which is of low cost and less volume, are stochastically modelled and analysed using Allan variance. Wavelet decomposition has been introduced to remove the high frequency noise that affects the sensors to obtain the original values of angular rates and accelerations with less noise. This increases the accuracy of the strapdown INS. The results show the effect of errors in the output of sensors, easy interpretation of random errors by Allan variance, the increase in the accuracy when wavelet decomposition is used for denoising inertial sensor raw data.

Keywords: Error modelling, Allan variance, wavelet decomposition, microelectromechnical systems, MEMS, inertial measurement unit, IMU, strapown inertial navigation system

NOMENCLATURE

ω_{mi}	Measured angular rate along each axis
ω_{ti}	True angular rate along each axis
α_{mi}	Measured acceleration along each axis
α_{ti}	True acceleration along each axis
$\overline{\Omega}(t)$	Cluster average
$\sigma^2(T)$	Allan variance of length T

1. INTRODUCTION

The inertial navigation system (INS) calculates velocity and position by integration of the total acceleration of the aircraft and integration of the resultant velocity, respectively. The strapdown INS eliminates most of the mechanical complexities of the gimbaled INS by having the sensors attached rigidly to the body of the aircraft, for the benefits of lower cost, reduced size, greater reliability, etc. The strapdown INS consists of inertial measurement unit (IMU) and navigation processor which computes position, velocity, and attitude based on navigation algorithm. The IMU consists of three accelerometers and three gyroscopes that provide accelerations along three axes and angular rates about three axes. The cost of strapdown INS is mainly determined by the IMU.

The cost and the volume of these inertial sensors can be drastically reduced using microelectromechnical systems technology. The fabrication processes of MEMS sensors make these very sensitive to the changes in the surrounding environmental conditions like temperature, pressure, electric, and magnetic fields, etc. These changes cause the output of MEMS sensors to vary rapidly, widely and sometimes randomly which make it difficult to appropriately model such variations. This high sensitivity to the surrounding environmental conditions adds more error types and possibly, higher errors than those of traditional non-MEMS sensors. Unless those errors are categorised, modeled and determined utilising special algorithms or techniques, the overall performance of MEMS sensors will be degraded when used in different applications, particularly inertial navigation. Inherent errors in the MEMS sensors are modelled. Allan variance is a method of representing root mean square (RMS) random drift error as a function of average time. It is easy to compute and relatively simple to read and understand. Allan variance method can be used to determine the character of the underlying random processes that give rise to the data noise. Allan variance method is used to characterise various types of noise terms in the MEMS inertial sensor data by performing certain operations on the entire length of data. The wavelet multi-resolution analysis (WMRA) technique has been suggested in this paper as an efficient pre-filter for MEMS-based inertial sensors outputs. Applying wavelet decomposition successfully improves the sensors' signal-to-noise ratios, removes short-term errors mixed with motion dynamics, and provides more reliable data.

2. MEMS INERTIAL SENSOR ERROR MODELLING

Modelling the errors in INS is one of the prominent topics in the field. The propagation of these sensor errors through the INS computations determines the accuracy of

Received 14 February 2009

the position, velocity, and orientation output of the INS. Error models are often used to analyse the performance of an INS from a given set of sensors. Conversely, it may be important to find out how accurate sensors need to be to obtain desired INS performance specifications. Here, error models of accelerometer triad and gyroscope triad are presented. Angle (velocity) random walk, bias stability, rate random walk, drift rate ramp, exponentially correlated (Markov) noise have been modelled as random noise.

2.1 MEMS Gyroscope Triad Error Modelling

The error model for three gyroscopes is represented as Eqn (1).

$$\begin{pmatrix}\omega_{mi}\\ \omega_{my}\\ \omega_{mz}\end{pmatrix}=\begin{pmatrix}Sb_x & M_{xy} & M_{xz}\\ M_{yx} & Sb_y & M_{yz}\\ M_{zx} & M_{zy} & Sb_z\end{pmatrix}\begin{pmatrix}\omega_{ti}\\ \omega_{ty}\\ \omega_{tz}\end{pmatrix}+\begin{pmatrix}G_{xx} & G_{xy} & G_{xz}\\ G_{yx} & G_{yy} & G_{yz}\\ G_{zx} & G_{zy} & G_{zz}\end{pmatrix}\begin{pmatrix}a_x\\ a_y\\ a_z\end{pmatrix}+\begin{pmatrix}G^2{}_x a_x a_z\\ G^2{}_y a_y a_z\\ G^2{}_z a_z a_y\end{pmatrix}+\begin{pmatrix}b_x\\ b_y\\ b_z\end{pmatrix}+\begin{pmatrix}Tb_x\\ Tb_y\\ Tb_z\end{pmatrix}+\begin{pmatrix}\eta_x\\ \eta_y\\ \eta_z\end{pmatrix} \quad (1)$$

where

ω_{mi} is measured angular rate along each axis,

ω_{ti} is true angular rate along each axis,

a_i is acceleration along each axis,

S_i is scale factor error along each axis,

M_{ij} is misalignment error along each axis,

G_{ij} is g-sensitive drift between two axes

$G^2{}_i = g^2$ is sensitive drift along each axis,

b_i is bias error along each axis,

Tb_i is temperature based drift along each axis, and

η_i is random noise along each axis.

2.2 MEMS Accelerometer Triad Error Modeling

The error model for accelerometer triad is represented as Eqn (2):

$$\begin{pmatrix}a_{mx}\\ a_{my}\\ a_{mz}\end{pmatrix}=\begin{pmatrix}S_x & M_{xy} & M_{xz}\\ M_{yx} & S_y & M_{yz}\\ M_{zx} & M_{zy} & S_z\end{pmatrix}\begin{pmatrix}a_{tx}\\ a_{ty}\\ a_{tz}\end{pmatrix}+\begin{pmatrix}b_x\\ b_y\\ b_z\end{pmatrix}+\begin{pmatrix}Ta_x\\ Ta_y\\ Ta_z\end{pmatrix}+\begin{pmatrix}A_{CGx}\\ A_{CGy}\\ A_{CGz}\end{pmatrix}+\begin{pmatrix}\eta_x\\ \eta_y\\ \eta_z\end{pmatrix} \quad (2)$$

where

a_{mi} *is* measured acceleration along each axis,

a_{ti} is true acceleration along each axis,

S_i is scale factor error along each axis,

M_{ij} is misalignment error along each axis,

A_{CGi} is acceleration due to CG offset along each axis,

b_i is bias error along each axis, and

Ta_i is temperature based drift along each axis.

The gyroscope triad and accelerometer triad error models are implemented using MATLAB. Figures 1 and 2 show the true angular rates and accelerations the aircraft experiences. These angular rates and accelerations are given as input to the above equations. Because of above-mentioned errors, the measurements from gyroscope triad and accelerometer triad are shown in Figures 3 and 4.

3. ERROR ANALYSIS OF INERTIAL SENSORS USING ALLAN VARIANCE

3.1 Allan Variance

Allan variance is a method of representing RMS random drift error as a function of average time. It is simple to compute and relatively simple to interpret and understand. Allan variance method is used to characterise various types of noise terms in the inertial sensor data by performing certain operations on the entire length of data. By performing these simple operations, a characteristic curve is obtained whose inspection provides systematic characterisation of various random errors present in the inertial sensor output data.

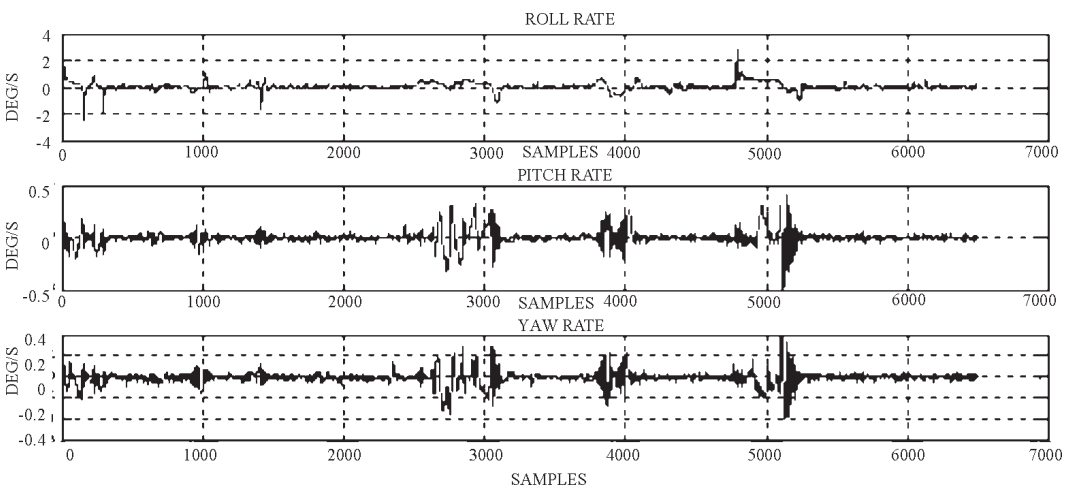

Figure 1. True angular rates about three axes.

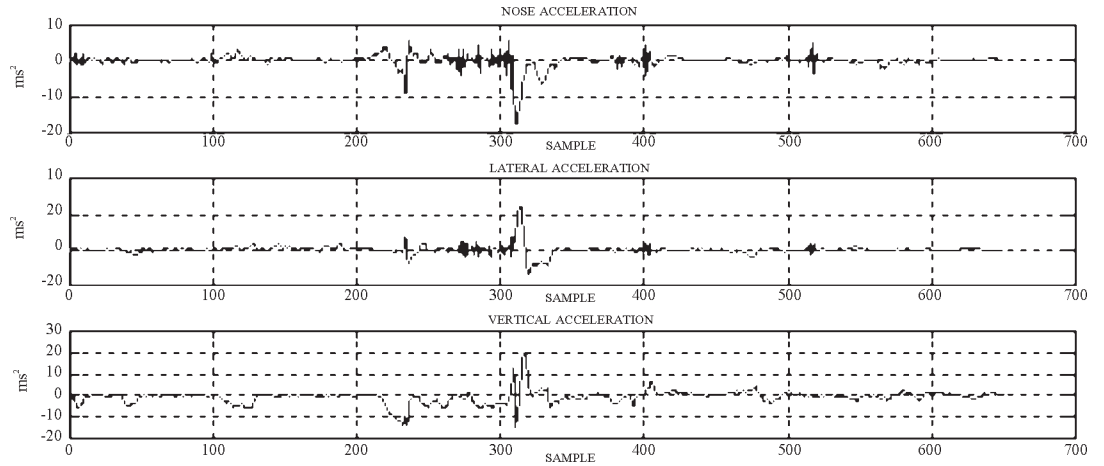

Figure 2. True accelerations along three axes.

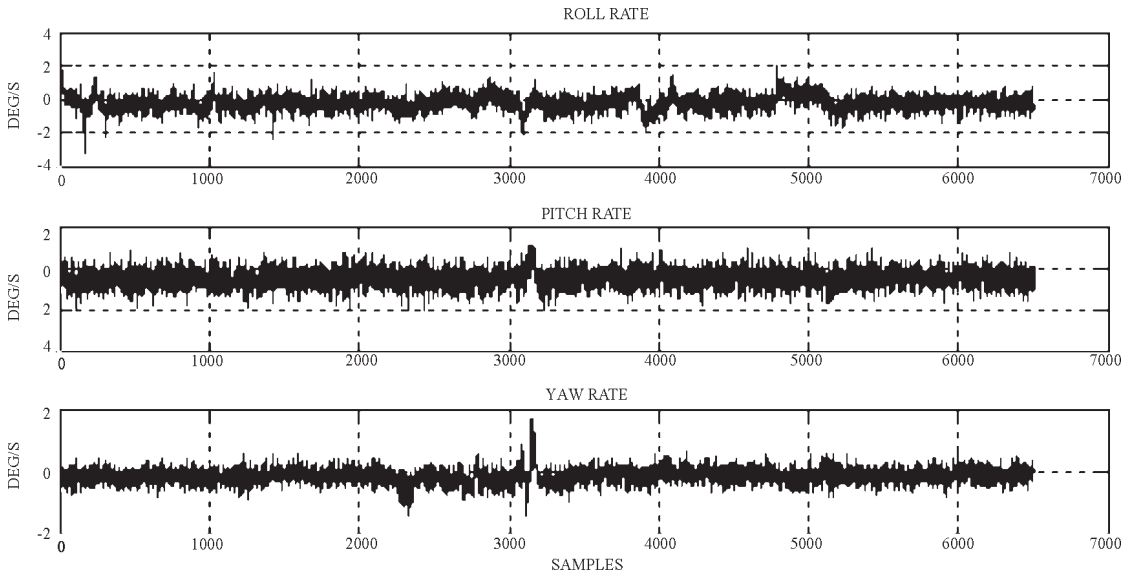

Figure 3. Raw output of three MEMS gyroscopes.

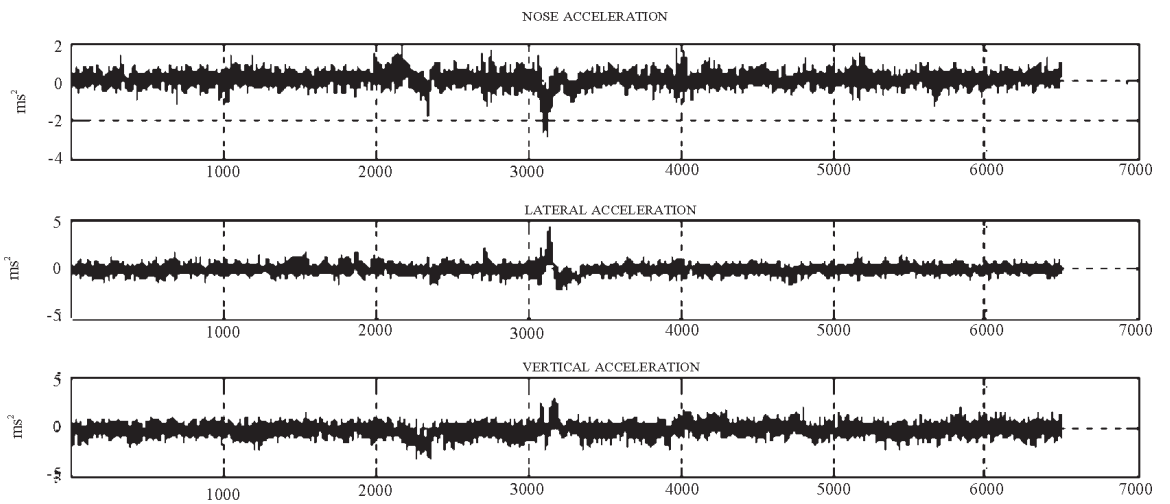

Figure 4. Raw output of three MEMS accelerometers.

3.2 Methodology

Allan variance is based on the method of cluster analysis. The steps involved in computing the Allan variance are:

(a) A data stream is divided into clusters of specified length. Assume there are *N* consecutive data points, each having a sample time of t_0. Forming a group of *n* consecutive data points (with $n<N/2$), each member of the group is a cluster, as shown in Fig. 5.

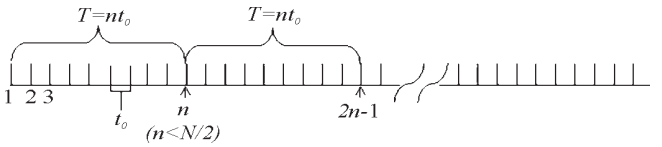

Figure 5. Schematic of the data structure used in the derivation of allan variance.

(b) Associated with each cluster is a time, *T*, which is equal to nt_0. If the instantaneous output rate of inertial sensor is $\Omega(t)$ the cluster average is defined as

$$\overline{\Omega}_K(t) = \frac{1}{T}\int_{t_k}^{t_k+T} \Omega(t)dt \tag{3}$$

where $\overline{\Omega}_K(t)$ represents the cluster average of the output rate for a cluster which starts from the k^{th} data point and contains *n* data points. The definition of the subsequent cluster average is

$$\overline{\Omega}_{next}(t) = \frac{1}{T}\int_{t_{k+1}}^{t_{k+1}+T} \Omega(t)dt \tag{4}$$

where $t_{k+1}=t_k+T$

(c) Performing the average operation for each two adjoining clusters and form the differences

$$\xi_{k+1,k} = \overline{\Omega}_{next}(t) - \overline{\Omega}_k(t) \tag{5}$$

For each cluster time *T*, the ensemble of defined by Eqn(5) forms a set of random variables. The quantity of interest is the variance of σ *s* over all the clusters of the same size that can be formed from entire data.

(d) Thus, the Allan variance of length *T* is defined (IEEE Std 952-1997) as:

$$\sigma^2(T) = \frac{1}{2}\left\langle\left[\overline{\Omega}_{next}(t) - \overline{\Omega}_k(t)\right]^2\right\rangle \tag{6}$$

The brackets in Eqn. (6) denote the averaging operation over the ensemble of clusters. Thus, above equation can be rewritten as:

$$\sigma^2(T) = \frac{1}{2(N-2n)}\sum_{k=1}^{N-2n}\left[\overline{\Omega}_{next}(t) - \overline{\Omega}_k(t)\right]^2 \tag{7}$$

Clearly, for any finite number of data points (*N*), a finite number of clusters of a fixed length (*T*) can be formed. Hence, Eqn (7) represents an estimation of the quantity $\sigma^2(T)$ whose quality of estimate depends on the number of independent clusters of a fixed length that can be formed.

3.3 Representation of Noise Terms in Allan Variance

The following sub-sections will show the integral solution for a number of specific noise terms, which are known to exist in the inertial sensor data:

(a) *Quantisation noise*: Allan variance for quantisation noise is given by

$$\sigma^2(T) = \frac{3Q_z^2}{T^2} \tag{8}$$

Where, Q_z is the quantisation noise coefficient and *T* is the sample interval. Therefore the root Allan variance of the quantisation noise when plotted in a log-log scale is represented by a slope of–1.

(b) *Angle (velocity) random walk*: High frequency noise terms, that have correlation time, much shorter than the sample time can contribute to the gyro angle (or accelerometer velocity) random walk. The Allan variance for angle (velocity) random walk becomes

$$\sigma^2(T) = \frac{Q^2}{T} \tag{9}$$

Eqn (9) indicates that a log-log plot of $\sigma^2(T)$ versus *T* has a slope of –1/2.

(c) *Bias instability*: The origin of this noise is the electronics, or other components susceptible to random flickering. Because of its low-frequency nature, it shows as the bias fluctuations in the data. Allan variance for bias instability:

$$\sigma^2(T) = \left(\frac{B}{0.6648}\right)^2 \tag{10}$$

Hence, the bias instability value can be read off the root Allan variance plot at the region where the slope is zero.

(d) *Sinusoidal noise*: The Allan variance for sinusoidal noise is given by

$$\sigma^2(T) = \omega_0^2\left(\frac{\sin^4(\pi f_0\tau)}{(\pi f_0\tau)^2}\right)^2 \tag{11}$$

Thus, the root Allan variance of a sinusoid when plotted in log-log scale would indicate sinusoidal behaviour with successive peaks attenuated at a slope of–1.

(e) *Rate random walk*: This noise is a result of integrating wideband acceleration PSD. This is a random process of uncertain origin, possibly a limiting case of an exponentially correlated noise with a very long correlation time. The Allan variance of rate random walk is

$$\sigma_{rrw}^2(f) = \left(\frac{K^2}{3}\right)\tau \tag{12}$$

This indicates that rate random walk is represented by a slope of + 1/2 on a log-log plot $\sigma(\tau)$ of versus τ. The unit of *K* is usually given in deg/h^2/(Hz)$^{1/2}$.

(f) *Rate ramp*: This is more of a deterministic error rather than a random noise. It could also be due to a very small acceleration of the platform in the same direction and persisting over a long period of time. Allan variance

of rate ramp is given by

$$\sigma_{rr}^2(\tau) = \frac{R^2\tau^2}{2} \quad (13)$$

This indicates that the rate ramp noise has slope of + 1 in the log-log plot of $\sigma(\tau)$ versus τ.

3.4 Sample Plot of Allan Variance

In general, any number of random processes discussed above can be present in the data. Thus, a typical Allan variance plot looks like the one shown in Fig. 6. This allows easy identification of various random processes that exist in the data. With real data, gradual transitions would exist between different Allan standard deviation slopes. A certain amount of noise or hash would exist in the plot curve due to the uncertainty of the measured Allan variance.

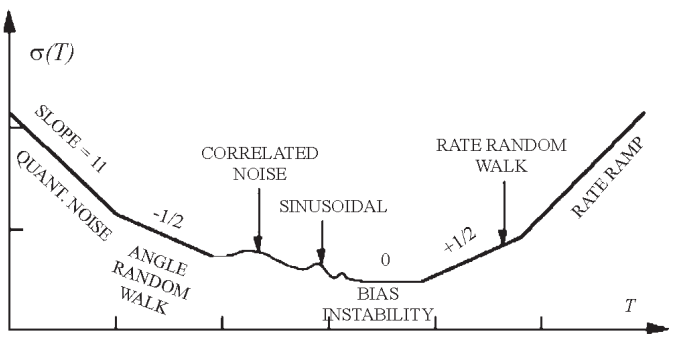

Figure 6. Sample Allan variance plot.

Figures 7 and 8 show the Allan variance plot for three gyroscopes and three accelerometers. When examining these figures it can be concluded that quantisation noise is dominant as the slope is -1 at less correlation time in all these sensors. When correlation time increases angle random walk becomes dominant, this is represented by a slope of –1/2 in Allan variance plot. As the correlation time further increases, the bias instability noise is observed by the zero slope in the Allan variance plot. The sinusoidal noise is observed by the variation in slopes, as shown in sample Allan variance plot.

The estimated noise coefficients for gyroscopes and accelerations from the Allan variance plot (Figs 7 & 8) are given in Tables 1 and 2.

Table 1. Identified noise coefficients for gyroscopes

	Quantization arc (s)	Angle random walk deg/h$^{1/2}$
Roll rate gyro	$5.4\text{x}10^{-4} \pm 1.48\text{x}10^{-5}$	$5\text{x}10^{-4} \pm 1.67\text{x}10^{-7}$
Pitch rate gyro	$4.32\text{x}10^{-4} \pm 1.16\text{x}10^{-5}$	$6\text{x}10^{-5} \pm 2\text{x}10^{-5}$
Yaw rate gyro	$3.6\text{x}10^{-5} \pm 9.72\text{x}10^{-7}$	$2.7\text{x}10^{-5} \pm 9\text{x}10^{-6}$

4. WAVELET DECOMPOSITION FOR DE-NOISING INERTIAL SENSOR DATA

Wavelets, as a mathematical tool, are based on analysing a signal through signal windowing but with variable window size. This gives an advantage to wavelet in performing local analyses, i.e., analysing a localised portion of a large signal. This is possible since wavelets allow the use

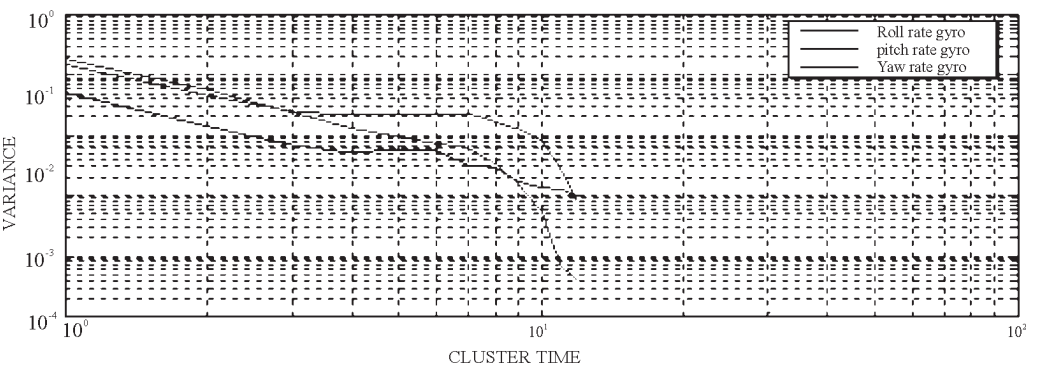

Figure 7. Allan variance plot for three gyroscopes.

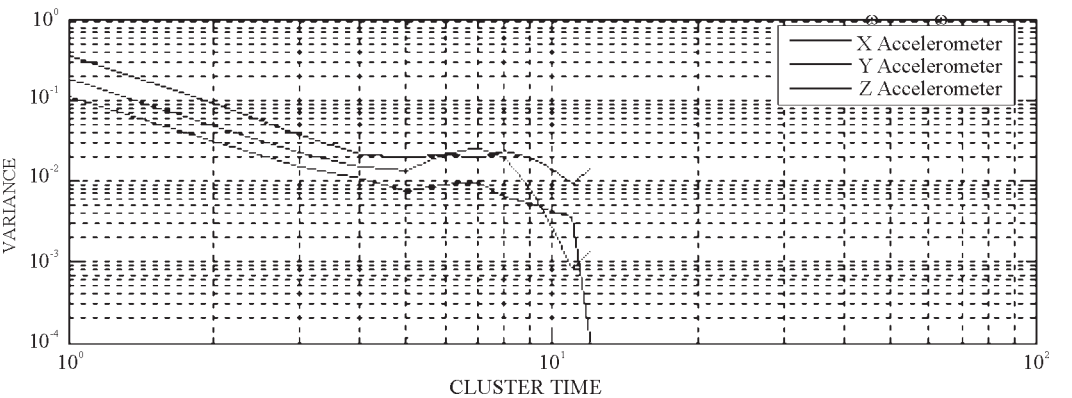

Figure 8. Allan variance plot for three accelerometers.

Table 2. Identified noise coefficients for accelerometers

Accelerometer	Quantisation (m/h)	Velocity random walk (m/s/$\sqrt{}$ h)	Rate random walk (m/s/h/$\sqrt{}$ h)
X	$5.4x10^{-5} \pm 1.458x10^{-6}$	$1.5x10^{-5} \pm 5x10^{-6}$	4.5 ± 1.5
Y	$1.26x10^{-3} \pm 3.4x10^{-5}$	$1.5x10^{-3} \pm 5x10^{-4}$	4 ± 1.33
Z	$9x10^{-5} \pm 2.43x10^{-6}$	$1.5x10^{-3} \pm 5x10^{-4}$	1.5 ± 0.5

of narrow windows (short-time intervals) for high frequency information and wide windows (long-time intervals) if low frequency information is needed.

4.1 Wavelet Multiple Level of Decomposition (Multi-Resolution Analysis)

In the implementation of the discrete wavelet transform (DWT), the wavelet coefficients of a signal are computed by passing it through two complementary half-band filters: a low-pass (LPF) filter and a high-pass filter (HPF). Therefore, the input signal will be decomposed into two parts. The first part will be the output of the HP filter (i.e., the details) while the second part will be the output of the LP filter (i.e., the approximation), (Fig. 9).

Based on the Nyquist theorem, if a signal has a sampling frequency of *fs*, the highest frequency component that the signal would represent is *fs*/2. By applying the DWT to decompose a signal and recalling that the LP and HP filters (shown in the filter bank of Fig. 9) have half-band characteristics, then the cutoff frequency of the LP filter is exactly at one-half of the maximum frequency appearing at the signal. Hence, if the DWT is applied on an inertial data of sampling frequency *fs*, the approximation part will include those inertial signal components that have frequencies of less than *fs*/4 while the details part will include the components of frequencies between *fs*/4 and *fs*/2. To obtain finer resolution frequency components of a specific signal, the signal is broken down into many lower-resolution components by repeating the DWT decomposition procedure with successive decompositions of the obtained approximation parts. This

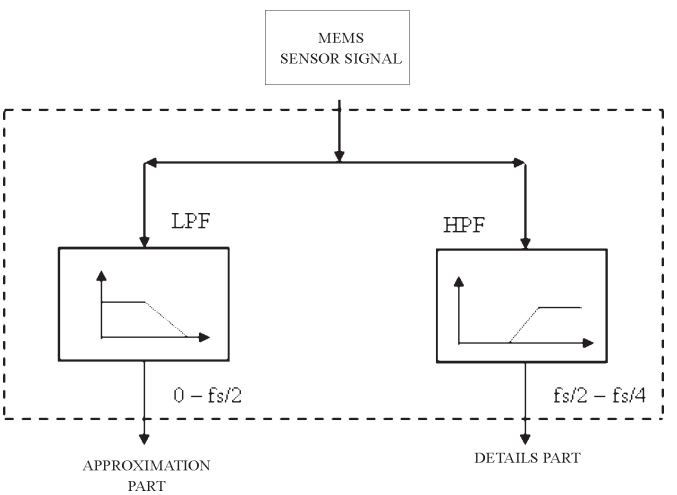

Figure 9. Signal decomposition by the discrete wavelet transform (DWT).

procedure is called either wavelet multiresolution analysis (WRMA) or wavelet multiple level of decomposition (LOD) or wavelet decomposition tree, as shown in (Fig. 10). However, this capability of representing a signal at several levels of resolution constitutes one of the powerful facilities of wavelets over other signal processing techniques. Using

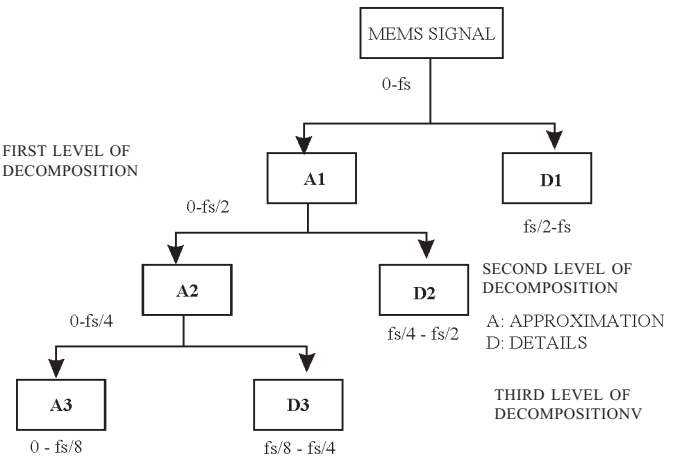

Figure 10.Wavelet multiresolution analysis considering three levels of decomposition.

WRMA, the signal can be represented by a finite sum of components at different resolutions, and hence, each component can be processed adaptively depending on the application at hand.

Practically, an appropriate multiple level of decomposition (LOD) is chosen based on the nature of the signal or on a specific criterion. Since noise is assumed to be zero mean, the wavelet decomposition level, at which the mean becomes non-zero, should be used for decomposition, since further decomposition would mean that actual trends in the data are being interpreted as noise. The Daubechies wavelet family provides the greatest degree of flexibility for parametric modifications involved in signal analysis. Here in this work, the Daubechies wavelet decomposition with the expected maximum wavelet LOD of level three has been applied for all the three MEMS gyroscopes and accelerometers raw data.

The results of the simulation of the wavelet decomposition using MATLAB are shown in Figs 11 and 12. From these results it is inferred that using wavelet decomposition, the high frequency components of noise are eliminated while the appropriate data of the inertial sensor contained in the low-frequency component is retained. The errors obtained

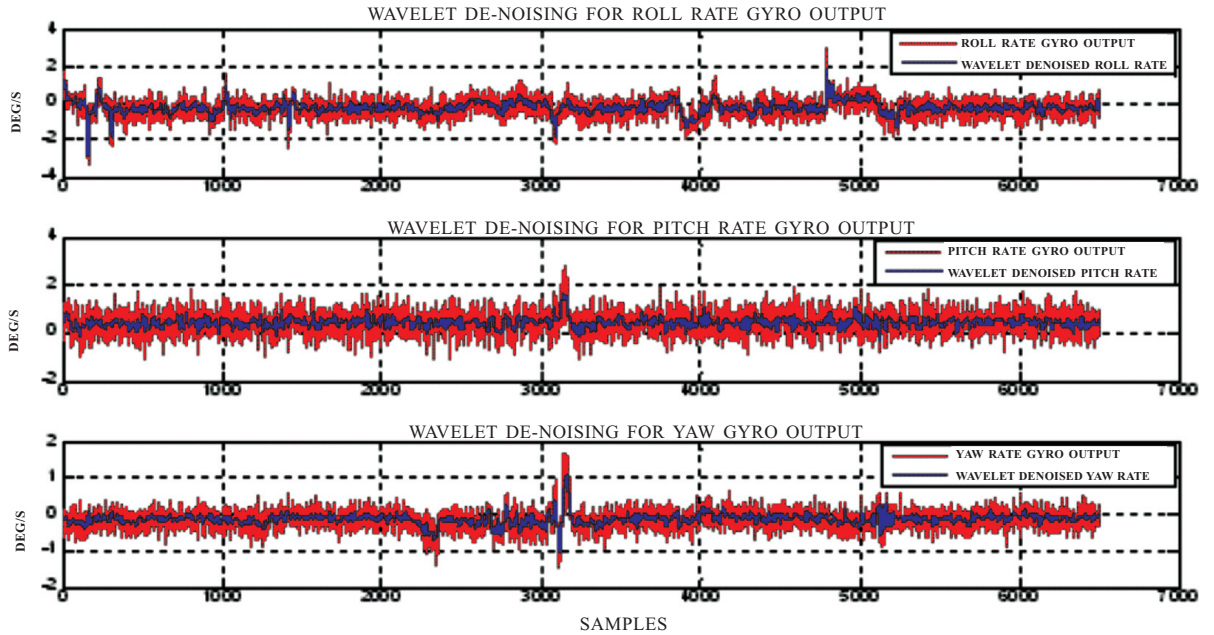

Figure 11. Wavelet de-noising of three MEMS gyroscopes raw output.

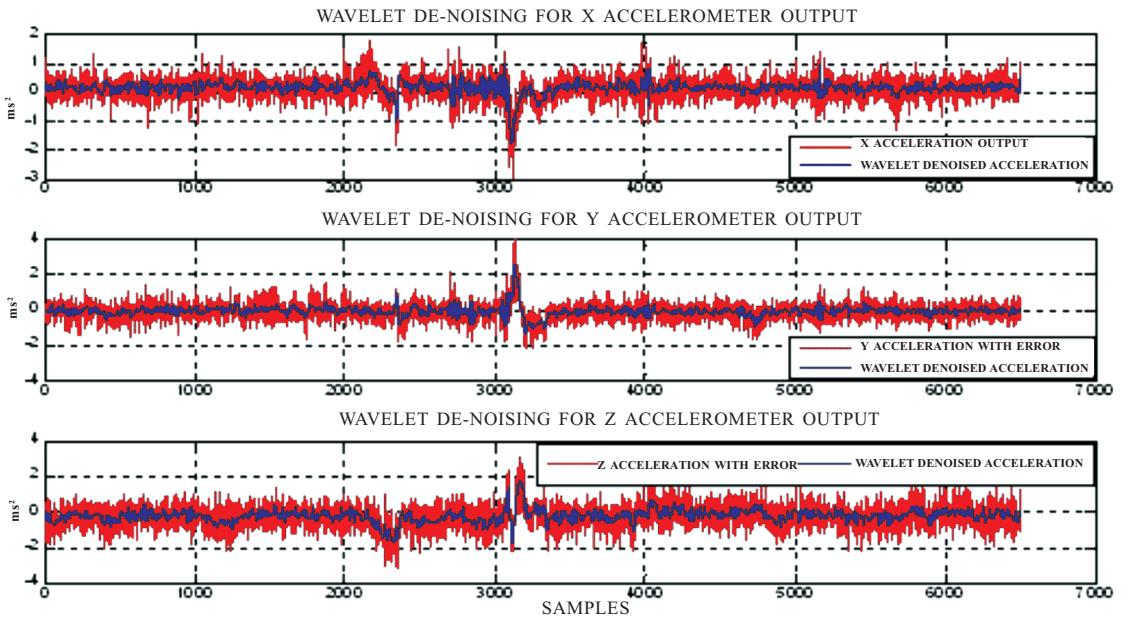

Figure 12. Wavelet de-noising of three MEMS accelerometers raw output.

using the original raw MEMS gyroscopes and accelerometers data (before de-noising) as well as the de-noised data with wavelet decomposition were computed. The statistics of such errors are given in Table 3 and the effectiveness of wavelet decomposition technique compared to a conventional LP filter is shown in Figs 13 and 14. It is evident that significant reduction in the measurement noise was achieved, thus reducing the measurement uncertainty.

The de-noising procedure was specifically beneficial in improving the SNR of pitch rate MEMS gyroscope measurement. Wavelet-based de-noising methods have the advantage over low-pass filtering in that relevant detailed information is retained, while small details due to noise are discarded.

Table 3. SNR values before and after de-noising

Parameters	Value				
Data points	1000	2000	3000	4000	5000
SNR dBs Before de-noising	4.2	4.25	4.4164	5.5495	4.09
SNR dBs After de-noising	17.726	17.567	18.34	19.105	18.818
Improvement in SNR	13.526	13.317	13.9236	13.5555	14.728

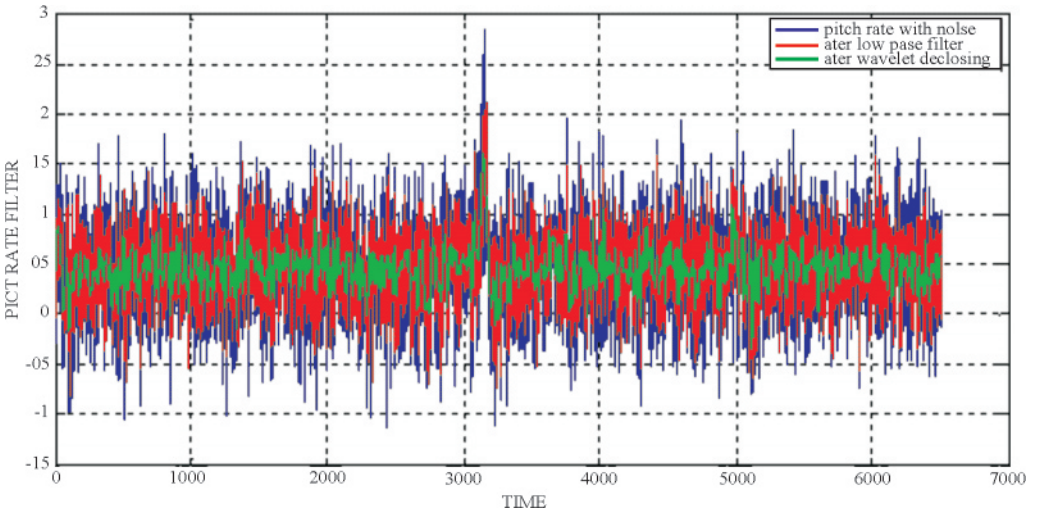

Figure 13. Wavelet de-noising and low-pass filter output of pitch rate MEMS gyroscope raw output.

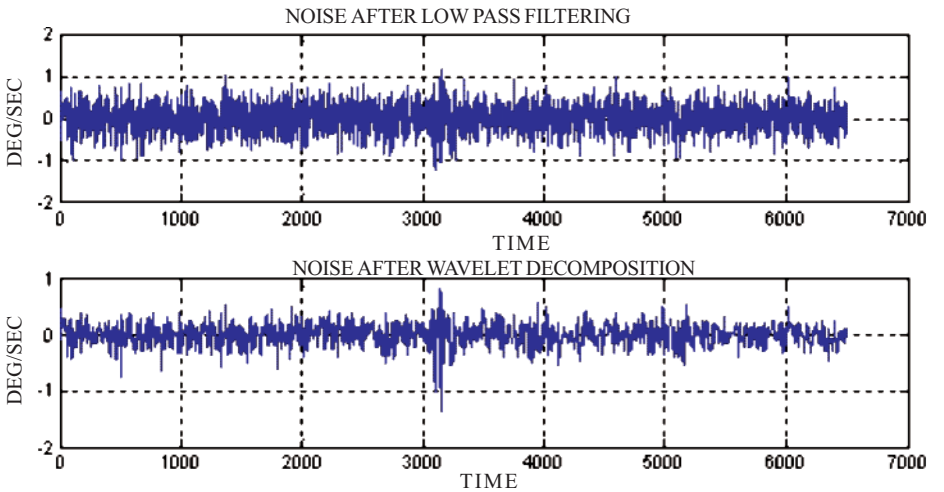

Figure 14. Noise after wavelet de-noising technique and low-pass filter of pitch rate MEMS gyroscope raw output.

5. CONCLUSIONS

The error models of MEMS accelerometer triad and gyroscope triad are presented including thermal drift. The errors have been analysed using Allan variance. It has been found that quantisation noise is the dominant noise at less correlation time, and as the time increases angle (velocity) random walk becomes dominant. The MEMS sensor output is de-noised using wavelet decomposition which improves the SNR which in turn increases the accuracy of the navigation. It has been observed that the high frequency component of noise is removed and signal is obtained with less noise.

REFERENCE

1. Aggarwal, Priyanka; Syed, Zainab; Niu, Xiaoji; & El-Sheimy, Naser. Cost-effective testing and caliberation of low cost MEMS sensors for integrated positioning, navigation and mapping systems. *In* XXIII FIG Congress, Munich, Germany, 2006.
2. Shantha Kumar, N . & Jann, T. Estimation of attitudes from a low-cost miniaturised inertial platform using Kalman filter-based sensor fusion algorithm. *Sadhana,* 2004, **29,** 217–235.
3. Ng, Lawrence C. On the application of Allan variance method for ring laser gyro performance characterisation. Report: Lawrence Livermore National Laboratory, 1993, Report No. UCRL-ID- 115695.
4. Goswami, J.C. & Chan, A.K. Fundamentals of wavelets: Theory, algorithms and applications. John Wiley & Sons Inc, 1999.
5. El-Sheimy, N.; Nassar, S. & Noureldin, A. Wavelet denoising for IMU alignment. *Aerspace Electro. Sys. Maga.*, 2004, **19**(10), 32-9.
6. Tian, Jin & Yang, Liu. A Novel GNSS weak signal acquisition using wavelet denoising method. *In* Proceedings of the 2008 National Technical Meeting of the Institute of Navigation, 28-30 January 2008. pp. 303-20.
7. Nassar, Sameh & El-Sheimy, Naser. Wavelet analysis for improving INS and INS/DGPS navigation accuracy.

Journal of Navigation, 2005, 119-34.

8. El-Sheimy, N.; Osman, A.; Nassar, S. & Noureldin, A. A new way to integrate GPS and INS: Wavelet multi resolution analysis. *GPS World,* **4**(10), 42-49.
9. Dolabdjiana, Ch.; Fadili, J. & Leyva, E. Huertas. Classical low-pass filter and real-time wavelet-based denoising technique implemented on a DSP: A comparative study. *Euro. Phy.: J. Appl. Phy.*, 2002.
10. Noureldin, Aboelmagd; Osman, Ahmed & El-Sheimy, Naser. A neuro-wavelet method for multi-sensor system integration for vehicular navigation. *Meas. Sci. Technol.*, 2004, **15**, 404-12.

Contributors

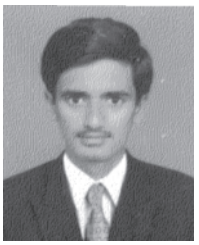

Mr R. Ramalingam obtained his BE (Electronics & Communication Engineering) in 2007 from Priyadharshini Engineering College, Vaniyambadi (Anna University) and ME (Avionics) in 2009 from Madras Institute of Technology (Anna University). Presently, he is working as Scientist B in Division of Avionics, (Aeronautical Development Establishment) ADE, Bangalore. His areas of interest include navigation systems and guidance.

Mrs G. Anitha obtained her BE (Electrical & Electronics Engineering) in 1997 from Alagappa Chettiar College of Engineering & Technology, MK University and her MTech (Control & Instrumentation) in 2003 from Indian Institute of Technology (IITM), Chennai. She is working as Lecturer in Avionics, Department of Electronics Engineering, MIT, Anna University, Chennai. Her areas of interest are: Navigation systems, guidance, and control and image processing.

Dr J. Shanmugam obtained his ME (Instrumentation Engineering), and PhD (Adaptive Control) from Anna University in 1983 and 1992, respectively. He is presently working as Principal at Velammal Engineering College, Chennai. His areas of interest are: Instrumentation, process control, avionics, navigation, and guidance and control.